Hindawi
Journal of Food Processing and Preservation
Volume 2023, Article ID 5288151, 15 pages
https://doi.org/10.1155/2023/5288151

Research Article

Flavonoids from Peony Seed Meal by Nanofiltration Membrane Separation

Ping Zou,[1] **Wentao Chen**,[1] **Ying Xu**,[1,2] **Yaohui Wang**,[2] **Yingyang Zhang**,[1] **and Rong Xu**[2]

[1]*School of Biological and Food Engineering, Changzhou University, Changzhou, Jiangsu 213164, China*
[2]*College of Petroleum and Chemical Engineering, Changzhou University, Changzhou, Jiangsu 213164, China*

Correspondence should be addressed to Ping Zou; zouping@cczu.edu.cn

Received 14 March 2023; Revised 7 July 2023; Accepted 26 July 2023; Published 10 August 2023

Academic Editor: Nadica Maltar Strmečki

Flavonoids are polyphenolic compounds with a wide range of biological activities (antioxidation, antitumor, and immunomodulatory). The membrane separation method of flavonoids has a high recovery and biological activity, overcoming the shortcomings of traditional methods for the separation of bioactive molecules. In this study, ethanol-water (*v*/*v*) solution was used to extract peony seed meal. The extraction rate of total flavonoids from peony seed meal was 35.28%. Five microfiltration membranes, polypropylene (PP), polyvinylidene fluoride (PVDF), cellulose acetate (CA), polyether sulfone (PES), and polyamide (PA), were selected to pretreat the extracts, and their separation performance was investigated. A new PA-supported silicone film was prepared by sol-gel method using 1,2-bis(TRIMETHOXYSILYL)ETHANE (BTESE) as a carrier. The synthesized BTESE/PA composite membrane was applied to the purification of organic silica PSMF solution by nanofiltration process. The optimal pressure of nanofiltration operation is 0.8 MPa, and the membrane flux can reach 2.06 $kg \cdot m^{-2} \cdot h^{-1}$. The mass concentration of flavonoids in the retention solution was decreased to 860.56 $mg \cdot L^{-1}$, and the permeable components of PSMF were effectively separated. The total flavonoid content of the purified lyophilized powder was 146.12 $mg \cdot g^{-1}$, which was 2.4 times that before purification. The results show that PSMF can be effectively separated by BTESE/PA membrane, and the membrane solution has good antioxidant activity.

1. Introduction

Peony is an economic and ornamental crop, which has been cultivated in China for more than 1600 years. Peony seed meal is one of the most important by-products in the preparation of peony seed oil, accounting for approximately 60~70% of peony seeds, which is also rich in flavonoids, proteins, polysaccharides, polyphenols, and other active ingredients [1, 2]. However, a large amount of oyster seed meal is currently used only as feed or waste, leading to waste of natural resources and environmental pollution.

In the process of agricultural food production, because many bioactive compounds with high value (such as phenolic compounds and anthocyanins) in the production process cannot be fully exploited and utilized, there is a great waste of resources. Here, specific value-added technologies, such as membrane-based processes, microwave, ultrasonic, pulsed electroassisted extraction, supercritical/subcritical fluids, and pressurized liquids, have emerged as advanced technologies for the extraction of various value-added biomolecules and have shown several advantages (improved extraction rates, reduced processing times, and protection of the bioactive properties of the compounds) [3]. With the continuous exploration of membrane technology, membranes overcome traditional methods (e.g., hot water extraction, solvent extraction, microwave-assisted extraction, adsorption, ultrasonic-assisted extraction, enzyme-assisted extraction, supercritical fluid extraction, and subcritical water extraction), most of the shortcomings in functional and bioactive molecular extraction [4]. By exposure to solvents, temperatures, and any other chemical agents, the bioactive molecules may degrade, resulting in inefficient recovery, and the process is not cost-effective due to the high rate of consumption of consumables (e.g., energy and solvents). Membrane technology is one of the ways to extract flavonoids. It is one of the most feasible methods for

recovering such compounds, with high recovery rates and minimal degradation. Other waste midmembranes can also recover small phenolic and protein components [5]. Zou et al. [6] used membrane separation to remove ginkgo toxin from ginkgo seed powder. Nazir et al. [7] applied membrane separation to recover nutrients from fruits, dairy products, grains, seafood, and slaughterhouse processing waste, enabling the sustainable production of nutraceuticals. Zhang et al. [8] explored membrane separation to extract light-colored lignin for preparing lignin nanoparticles as UV sunscreen. Organically bridged silica is a promising material for application in molecular separation membranes. Castricum et al. [9] prepared the microporous organosilica membrane by hydrolysis and polymerization reaction of 1,2-bis(-triethoxysilyl)ethane (BTESE) and applied it to pervaporation dehydration of n-butanol [10]. Afterward, the applications of BTESE-derived organosilica membranes have expanded to reverse osmosis, gas separation, and nanofiltration processes [11]. Two valuable flows obtained from membrane treatment are permeation flow and entrapment flow. The osmotic flow consists of a solvent passing through the membrane and has an abundance of solutes at the nominal molecular weight cutoff value (NMWCO) of the membrane [12]. Pressure-driven membranes such as microfiltration (MF), ultrafiltration (UF), and nanofiltration (NF) processes offer several advantages: low energy requirements, high separation efficiency, ease of amplification, simple operation, high permeability flux productivity, and no phase transitions. In general, these advantages promote the recycling of high-value-added components. The performance of pressure-driven membrane technology usually depends on the operating conditions (TMP, flow rate, and temperature), but in addition to this, for these types of processes, a number of other factors. For example, the type of membrane and its properties (MWCO, membrane material, hydrophilic or hydrophobic, structure, module configuration, material, porosity, and surface charge) also play an important role [13]. Depending on the membrane material, the membrane surface of reverse osmosis, nanofiltration, and ultrafiltration membranes is usually negatively charged depending on the presence of sulfonic acid or carboxyl groups [14, 15]. These groups are related when using zwitterions, which are defined as molecules that have two or more functional groups, at least one of which has a positive charge and one that has a negative charge so that the net change across the molecule becomes zero. In principle, specific forces such as electrostatic repulsion tend to occur when the contaminant and membrane display the same charge, and the presence of this molecule reduces this phenomenon. Few studies have recognized that some bacterial solutions carry a negative charge, so if the membrane is negatively charged, it shows less likelihood of adhesion than the possibility of being positively charged [16]. Based on this statement, chemical modification of membranes by zwitterions has emerged as a promising alternative. Organic bridged silica is a promising membrane material for molecular separation. Subsequently, the application of BTESE-derived organic silica membranes was expanded to reverse osmosis, gas separation, and nanofiltration processes [17, 18].

In this study, we present the first results on the development of polyamide (PA) supported BTESE membrane for the purification of natural flavonoids by membrane-based nanofiltration. The peony seed meal was extracted by organic solvent extraction to obtain the crude extract of peony seed meal flavonoids (PSMF). Five types of microfiltration membranes, polypropylene (PP) [19], polyvinylidene fluoride (PVDF) [20], cellulose acetate (CA) [21], polyethersulfone (PES) [22], and polyamide (PA) [23], were selected for evaluating the effect of preliminary decontamination. The flavonoids in the extracts were analyzed by high-performance liquid chromatography (HPLC), and 12 fractions were maintained. Then, these fractions were further purified by the fabricated BTESE/PA composite membranes. Various characterizations were performed to provide the chemical-physical properties of these membranes, and the separation performances of the membranes were systematically evaluated.

2. Materials and Methods

2.1. Raw Materials. Material peony seed meal was purchased from Jiangsu Guose Tianxiang Oil Peony Technology Development Co. (Jiangsu, P. R. China). 1,2-bis(TRIMETHOXYSILYL)ETHANE (BTESE) was purchased from Aladdin Reagent Co. (Shanghai, P. R. China). Polypropylene (PP), polyvinylidene fluoride (PVDF), cellulose acetate (CA), polyethersulfone (PES), and polyamide (PA) were purchased from Haiyan New Oriental Plastic Technology Co. (Zhejiang, P. R. China), and the specific information of microfiltration membrane is shown in Table 1. Other chemicals used in this study were of chromatographical or analytical grade.

2.2. PSMF Extraction. The peony seed meal was crushed and passed through an 80 mesh sieve, and ethanol-water (*v*/*v*) solution was selected as the solvent to extract the natural flavonoids from the peony seed meal [24], and the supernatant was extracted by centrifugation. Single-factor experiments were conducted to determine the optimum conditions for PSMF extraction as follows: material-liquid ratio ($m_{\text{peony seed meal}} : V_{\text{ethanol}}$) $1:15\,g{\cdot}mL^{-1}$, extraction temperature 50°C, ethanol concentration 70%, extraction time 30 min, and the highest PSMF concentration $236.19\,mg{\cdot}L^{-1}$.

2.3. Pretreatment of PSMF Solution. Since PSMF extracts are obtained by heating in solution, which is hot and contains impurities, for this reason, five materials [19–23] that are less prone to scaling and have good chemical and thermal stability were selected as the support for PSMF separation. Ideally, the naturally occurring harmful substances are removed while maintaining the antioxidant capacity of the extracts themselves. Under pressure, the extract of PSMF flows through the micropores on the membrane to the low-pressure measurement of the membrane as a microfiltration permeate, and particles larger than the membrane pore size are retained, thus achieving the separation of particles from the solvent in the raw material solution. The sample was measured at an operating pressure of 0.01 MPa, an operating temperature of 25°C, an effective membrane area

Table 1: Physical properties of membranes.

Sample	Pore size (mm)	Porosity (%)	Advantage	Shortcoming	Manufacturer
PP	0.22	40.3 ± 2.8%	Low density, good mechanical properties, easy to form.	Its hydrophobicity and surface inertia affect the practical application of some aspects, such as the surface being easy to cause protein and platelet adhesion and easily causing a bacterial infection.	Zhejiang, P. R. China
PVDF	0.22	57.2 ± 3.5%	It has good mechanical properties, film-forming properties, excellent corrosion resistance, and chemical stability.	It burns with fluorine smoke and is not easy to bond.	Zhejiang, P. R. China
CA	0.22	58.3 ± 2.5%	Rich source, low price, good film formation, and biocompatibility.	The elongation at break is lower under dry conditions, and the texture is brittle.	Zhejiang, P. R. China
PES	0.22	60.5 ± 3.0%	Excellent heat resistance, physical and mechanical properties, and insulation properties.	In the treatment of wastewater, the driving force is high and it is easy to pollute, thus reducing the separation efficiency, increasing the operating cost of equipment, and shortening the service life of the membrane.	Zhejiang, P. R. China
PA	0.22	57.2 ± 1.5%	Good mechanical properties, good wear resistance, good chemical stability, and strong solvent resistance.	Affected by temperature and water absorption, it has general weather resistance and poor thermal stability.	Zhejiang, P. R. China

of 6.10 cm^2, and a prepressure of 30 min on the microfiltration membrane. The permeate was lyophilized and preserved, and the best microfiltration membrane for the separation was determined based on the membrane flux of different types of microfiltration membranes, water contact angle, and the characterization of PSMF permeate lyophilized powder by scanning electron microscopy and thermogravimetry.

2.4. Preparation of BTESE/PA Composite Membrane

2.4.1. Synthesis of BTESE Sol. The precursor 1,2-bis(TRIMETHOXYSILYL)ETHANE (BTESE) was purchased from Aladdin Reagent Co., Ltd., and n-propanol (NPA) with a specification of 99.7% was chosen as the solvent to prepare the organosilica sols. The selected catalysts were HCl and NH_3, and two BTESE sols were prepared: acid-catalyzed and base-catalyzed. The molar ratio of BTESE/H_2O/HCl was 1/60/0.1, and the sols were prepared by hydrolysis with water and catalyst at 40°C for 2 h. The precursor concentration of both sols was kept at 5.0 wt%. BTESE sols were dried by vacuum drying oven at 100°C under an air atmosphere. Finally, BTESE powder was obtained by grinding with a mortar and pestle. The synthesis process of the sol is shown in Figure 1.

2.4.2. BTESE/PA Composite Membrane Preparation. Pretreatment of polymer PA supports: the polymer PA supports were cut into regular quadrilateral shapes and immersed in distilled water for at least 12 h to remove glycerol and impurities from the surface layer of the supports. After retrieval, the supports were fixed to a glass plate using high-temperature resistant tape to prevent curling around them and finally dried in a vacuum drying oven at 100°C for 5 min.

BTESE/PA composite membrane preparation: the BTESE solute solution was loaded on the PA membrane surface by spin coating. One of the key aspects of manufacturing homogeneous composite membranes is to ensure the uniform distribution of nanoparticles within the polymer matrix. The BTESE/PA composite membrane was prepared by spin coating the BTESE sol particles using a KW-4A benchtop homogenizer at 5000 rpm, where the PA spacer was fixed on a glass disk to prevent wrinkle formation, BTESE sol was added dropwise to the center of the spacer, and the spacer was moistened around it and then heat cured in a vacuum drying oven at 100°C for 10 min. A diagram of the BTESE silicone composite membrane prepared by the spin coating method is shown in Figure 2.

2.5. PSMF Permeation Vaporization Measurement. Figure 3 shows the schematic diagram of the PSMF nanofiltration through the permeate vaporization unit, thus achieving separation. Since the back side of the membrane is at low pressure, the components are vaporized into vapor as soon as they pass through the membrane, and the vapor is pumped away by vacuum to keep the permeate process going [25]. Each component of the stock solution passes through the membrane at a different rate, and the component that permeates through the membrane faster can be separated from the stock solution. The membrane flux was measured after prepressurizing the membrane for 30 min at an operating pressure of 0.8 MPa, an operating temperature of 25°C, and a flow rate of 9.99 mL·min^{-1}. The effective area of the membrane was 6.11 cm^2 unit, thus achieving separation. Since the back side of the membrane is at low pressure, the components are vaporized into vapor as soon as they pass through the membrane, and the vapor is pumped away by vacuum to keep the permeate process going [25]. Each component of the stock solution passes through the membrane at a different rate, and the component that permeates through the

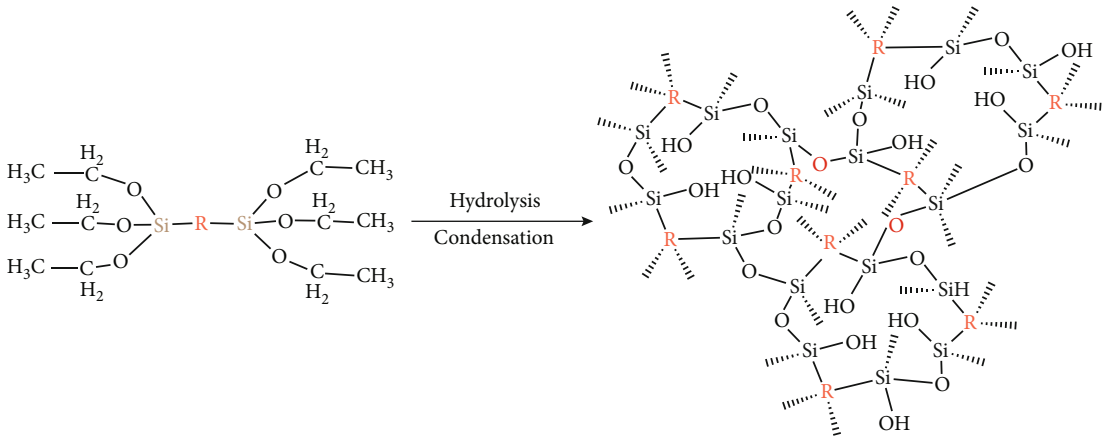

Figure 1: Schematic synthesis of BTESE sol.

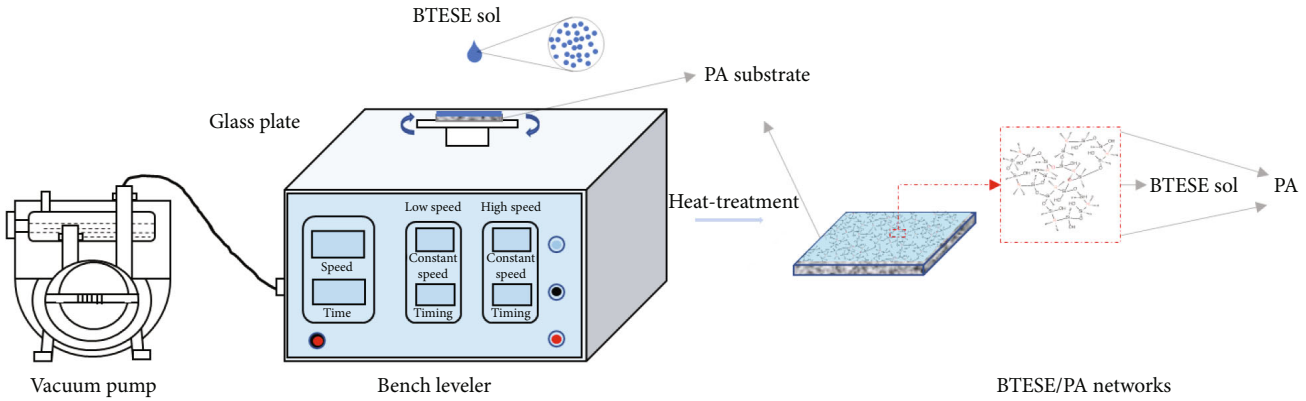

Figure 2: Schematic diagram of the preparation of the BTESE/PA composite membrane.

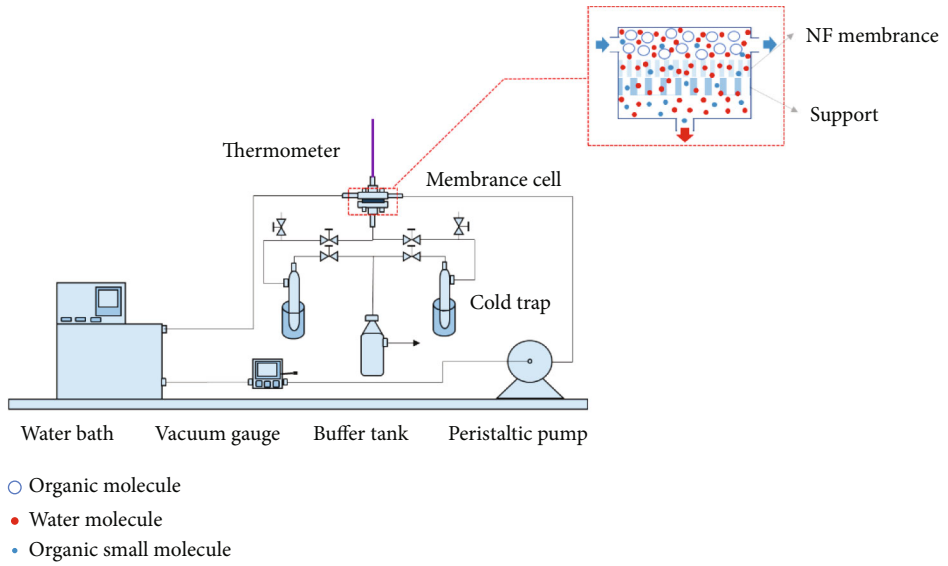

Figure 3: Schematic diagram of the nanofiltration process.

membrane faster can be separated from the stock solution. The membrane flux was measured after prepressurizing the membrane for 30 min at an operating pressure of 0.8 MPa, an operating temperature of 25°C, and a flow rate of 9.99 mL·min^{-1}. The effective area of the membrane was 6.11 cm^2.

Membrane flux (or transmission rate) is an important process operating parameter in the membrane separation process, and membrane flux was calculated by Equation (1) [26], which refers to the amount of fluid passing through the unit membrane area in a unit of time, generally expressed in m^3/(m^2·s) or L/(m^2·h) (or m/s).

$$J = \frac{V}{T \times A}, \tag{1}$$

where J is the membrane flux (L/m^2·h), V is the sampling volume (L), T is the sampling time (h), and A is the membrane effective area (m^2).

Retention rate is the ability of the membrane to prevent a component from passing through or retaining a component in the feed solution, and retention rate was calculated by the following equation [27, 28]:

$$R = \left(1 - \frac{C_1}{C_2}\right) \times 100\%, \tag{2}$$

where R is the retention rate, C_1 is the penetration concentration, and C_0 is the feed concentration.

At the end of the concentration phase, the membrane is cleaned with pure water at a fixed pressure (3 bar) for 1 hour. The flux recovery rate (FRR) used to evaluate the membrane cleaning effect was calculated by the following equation [29]:

$$\text{FRR} = \frac{Jw2}{Jw1} \times 100\%, \tag{3}$$

where $Jw2$ and $Jw1$ are, respectively, the membrane flux of PSMF mixed solution before and after cleaning.

2.6. Examination of PSMF. The detection was performed using a WATERS 515 ultrahigh performance liquid phase system (WATERS, USA) [30], which was repeated three times depending on the nature of the compounds, using Hyper 0DS2 C18 packing with mobile phase A being an 85% formic acid-water (v/v) solution and mobile phase B being a deionized water solution. The scavenging effect of PSMF on 1,1-diphenyl-2-picrylhydrazyl (DPPH) radicals, hydroxyl (OH) radicals, and superoxide anion (-O^{2-}) radicals before and after membrane separation was verified according to the literature [31, 32], as well as the determination of the reducing power.

2.7. Determination of Free Radical Scavenging Rate

2.7.1. OH· Scavenging Ability Assay. The mixture consisted of 4 mL 1,10-phenanthroline (5 mM) and 4 mL $FeSO_4$ (5 mM), then 3 mL phosphate buffer (16 mL 0.2 mol/mL sodium dihydrogen phosphate+84 mL 0.2 mol/mL disodium hydrogen phosphate configuration, pH = 7.4) was added, followed by 3 mL H_2O_2 (0.01%) and 4 mL PSMF sample solution, and the mixture was shaken well and allowed to stand for 1 h. The absorbance was measured at 536 nm. Control : distilled water was used instead of PSMF solution, and other reagents were the same as the samples. Blank : distilled water was used instead of hydrogen peroxide, and other reagents were the same as the samples. OH· scavenging rate is calculated by the following equation [33]:

$$\text{OH} \cdot \text{ scavenging rate} = \frac{A_i - A_j}{A_0 - A_j} \times 100\%, \tag{4}$$

where A_i, A_j, and A_0 represent the absorbance of the sample, control, and blank, respectively.

2.7.2. O_2^- Scavenging. Take 1.5 mL of sample solution, and then add 0.5 mL of 0.30 mmol/L NBT (pH 8.0 Tris-HCl preparation), 0.5 mL of 0.468 mmol/L NADH (pH 8.0 Tris-HCl preparation), and 0.5 mL of 0.060 mmol/L PMS (pH 8.0 Tris-HCl preparation), respectively, in order. The mixture was mixed well and then placed in a water bath at 25°C for 5 min. The absorbance at 560 nm was measured, and the O_2^- scavenging rate was calculated by the following equation [34]:

$$\cdot O_2^- \text{ scavenging rate} = \frac{1 - A_i}{A_0} \times 100\%, \tag{5}$$

where A_i and A_0 represent the absorbance of the sample and blank, respectively.

2.7.3. DPPH Scavenging Ability Assay. The samples were 2 mL of PSMF solution (50, 100, 150, 200, and 250 μg/mL) and 2 mL of 0.1 mM DPPH solution (dissolved in 95% ethanol). The blank was 95% ethanol 2 mL+0.1 mM DPPH 2 mL. The reaction was carried out at room temperature, protected from light for 30 min, and measured by a spectrophotometer at 517 nm. The DPPH clearance was calculated by the following equation [35]:

$$\text{DPPH scavenging rate} = \frac{A_0 - A_i}{A_0} \times 100\%, \tag{6}$$

where A_i and A_0 represent the absorbance of the sample and blank, respectively.

2.7.4. Reduction Power Measurement. Take 1 mL of sample solution, add 1 mL of 0.2 mol·L^{-1} phosphate buffer solution (62.5 mL of 0.2 mol·mL^{-1} sodium dihydrogen phosphate +37.5 mL of 0.2 mol·mL^{-1} disodium hydrogen phosphate configuration, pH = 6.6), then add 1% (w/v) potassium ferricyanide, heat in a water bath at 50°C for 20 min and then cool quickly, then add 1 mL of 10% (w/v) of the glacial acetic acid solution, mix well, centrifuge at 3000 r·min^{-1} for 10 min, then take 1.5 mL of supernatant and add 1.5 mL of distilled water and 1% (w/v) of ferric chloride, react for 10 min, and measure the absorbance at 700 nm, and the reducing power was expressed by the absorbance value.

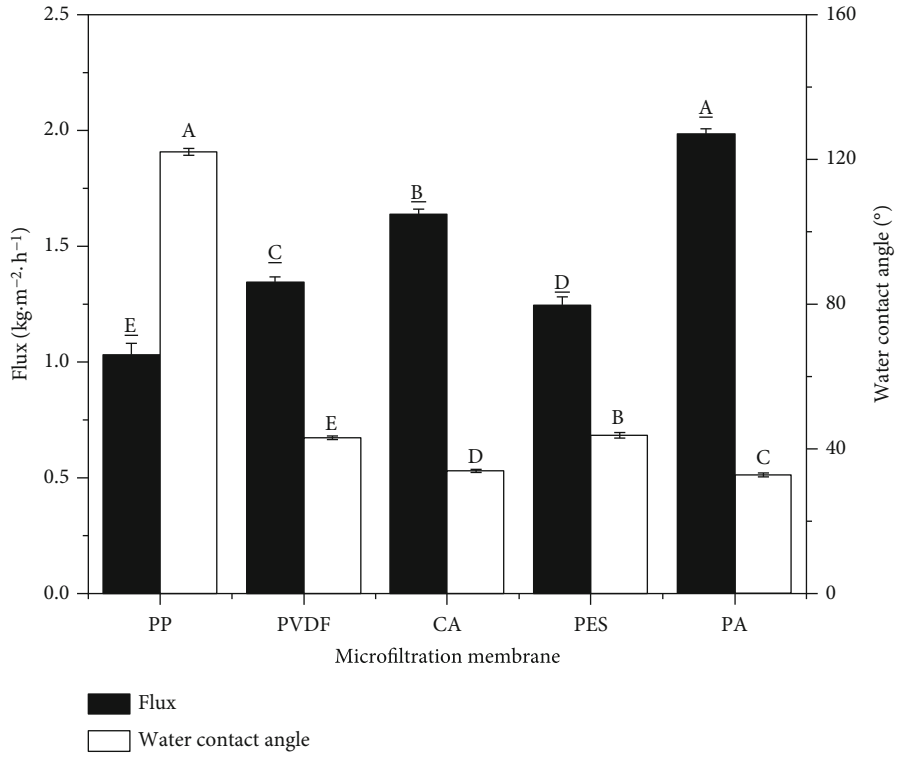

Figure 4: WCA of five microfiltration membranes.

2.8. Characterization Methods

2.8.1. Sol and Gel Analysis. The chemical composition of the composite membrane as well as the peritectic solution was analyzed by Nicolet iS50 Fourier infrared spectroscopy (FT-IR) at 25°C, and the content of each component of the mixture was deduced. The isothermal adsorption curves of BTESE sol-gel powder were determined by using a TG 209 F3 thermogravimetric analysis (TGA) from NETZSCH, Germany, with N_2 as the carrier gas and a gradual temperature increase to 800°C at 10°C·min^{-1}.

2.8.2. Membrane Performance. Calibrate the instrument using a ceramic calibration rod. When the temperature condition is 25°C, the surface tension value of deionized water is 71.97 mN/m, which meets the measurement requirements. A plate membrane with a size of 3 cm × 3 cm was taken, and the contact angle values of five types of microfiltration membrane surfaces were measured at multiple points using a water contact angle (WCA) meter. Solutions with low surface tension (small contact angle) have better wettability, which is beneficial for improving the film formation quality during the spin coating process.

After soaking the membrane with anhydrous ethanol for 3 seconds, the brittle fracture was placed in liquid nitrogen. Before observation, the sample was sprayed with gold. The surface and cross-sectional morphology were measured using a German Zeiss SUPRA 55 field emission scanning electron microscope (FE-SEM) at 15 kV, respectively.

The content of C, O, N, and Si in PA film and BTESE/PA composite film was measured using the S8 Tiger X-ray fluorescence spectrometer of Bruker AXS GmbH in Germany.

The surface roughness is less than 5 μm. The atomic force microscope (AFM) was used to analyze the morphology and nanostructure of the membrane surface in a dry atmosphere with a probe amplitude of 5 nm and obtain information about the size, pore diameter, material surface roughness, material surface defects, etc., of nanoparticles.

3. Results and Discussion

3.1. Characterization of 5 Types of Microfiltration Membranes. As shown in Figure 4, the water contact angles of PVDF, CA, PES, and PA are all less than 90°, indicative of the hydrophilic nature of the materials. Better surface hydrophilicity of the membrane typically suggested a high water flux[36], which was consistent with the experimental result that the lowest water flux for the PP membrane. For permeation of PSMF through the five membranes, the flux of the PA membrane was higher than those of the other four membranes, and the solution was transparent after passing the membrane, with less loss of active ingredients in the PSMF solution.

The surface and cross-sectional morphology of the membranes were observed using field emission scanning electron microscopy (FE-SEM, Zeiss, SUPRA 55), and the preparation of high-quality BTESE coatings on the relatively rough support surface was difficult compared to the smooth

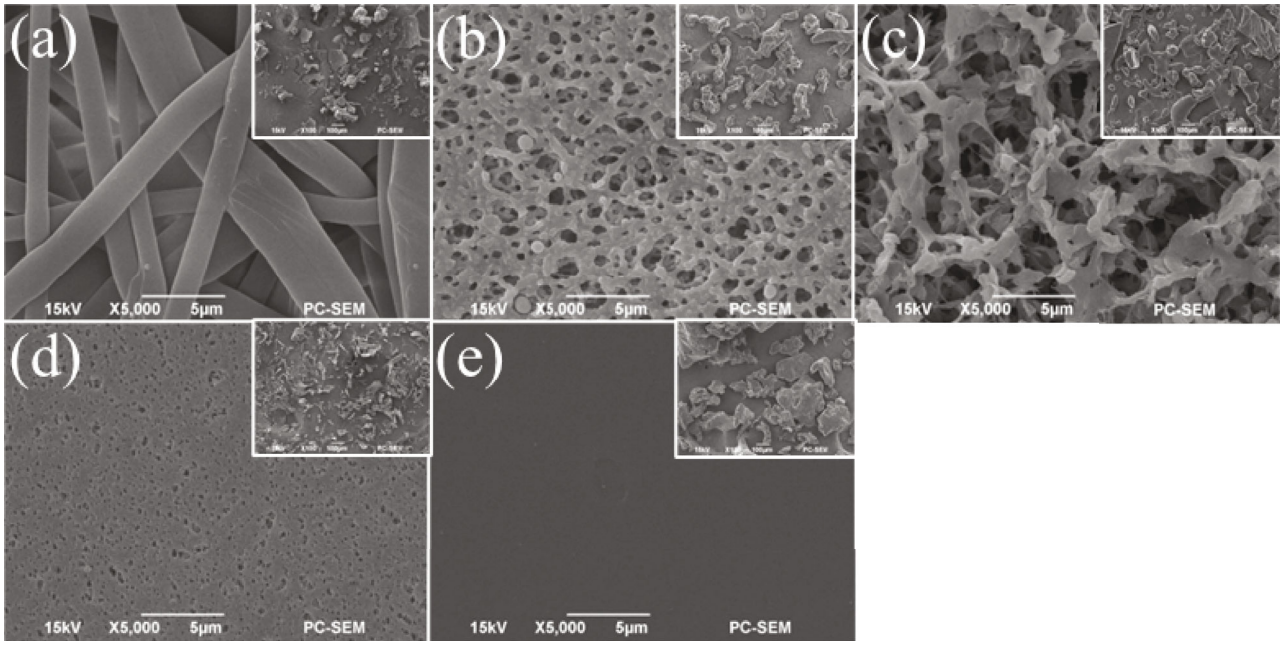

Figure 5: SEM images of the microfiltration membranes (inserted chart is SEM of PSMF membrane solution lyophilized): (a) PP, (b) PVDF, (c) CA, (d) PES, and (e) PA.

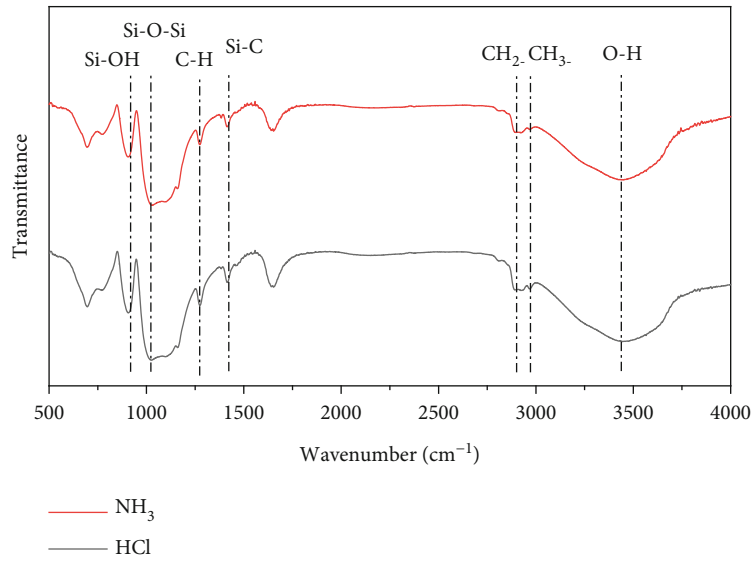

Figure 6: FT-IR of BTESE.

support [37]. As shown in Figure 5, from the SEM images of five types of microfiltration membranes, it could be observed that the surface of the PA membrane was smoother than the other four membranes. Inserts were the SEM image of the freeze-dried samples of PSMF solution on the permeate side of the membranes, and the lyophilized particles of PSMF solution are more homogeneous after passing through the PA membrane. Therefore, PA is preferred as a support for the preparation of the composite membranes.

3.2. BTESE Sol Preparation and Characterization. BTESE sols were prepared by two routes: acid-catalyzed and base-catalyzed. The BTESE dry gel powder (dried at 100°C) was well ground with potassium bromide powder, pressed into tablets, and put into an FTIR spectrometer (Nicolet iS50), and the chemical structure of the samples was characterized, as shown in Figure 6. It is clear from the figure that all dry gels have a strong Si-OH stretching vibration peak at around 920 cm^{-1}. Meanwhile, the peak at 1020-1200 cm^{-1} is a stretching vibration peak of Si-O-Si, which confirms the successful hydrolysis and condensation during the sol-gel process. The results reveal that the peak intensities of the Si-OH and Si-O-Si groups of the BTESE dry gels prepared by the two methods are similar; the telescopic vibrational peak of Si-C at 1430 cm^{-1} indicates that organosilica is formed in all sol-gel structure in all sols, and since both use n-

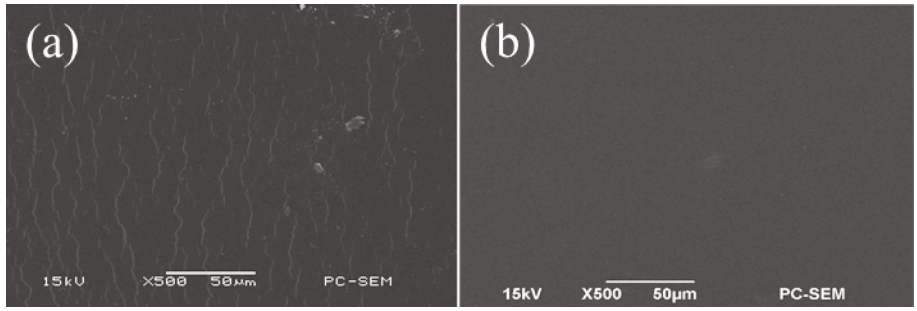

Figure 7: SEM of BTESE: (a) NH3; (b) HCl.

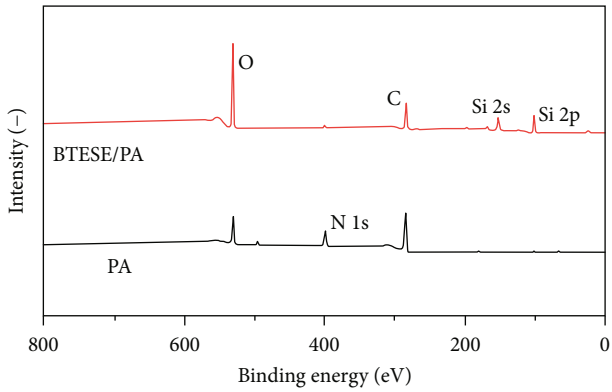

Figure 8: XPS spectrum of PA support and BTESE/PA composite membrane.

Table 2: Surface element abundance analysis of PA support and BTESE silica composite membrane.

Membranes	C%	N%	O%	Si%
PA	67.21	13.24	19.55	
BTESE/PA	30.13		34.93	34.94

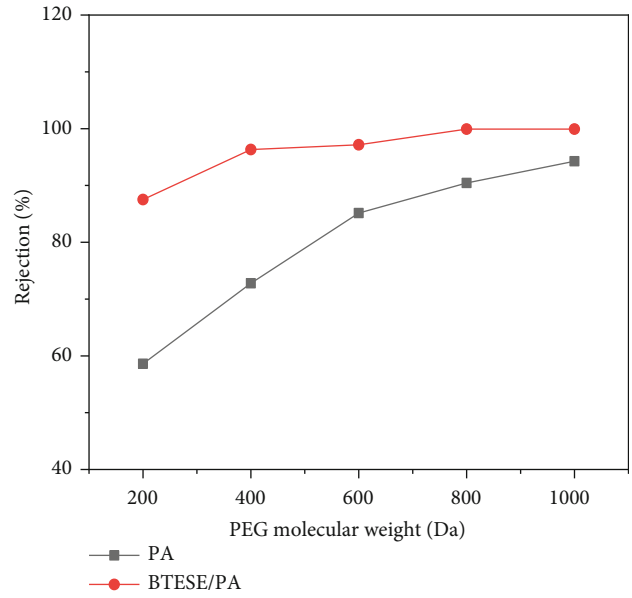

Figure 9: Molecular weight determination of PA and BTESE/PA (PA, 5 wt% BTESE, 25 ± 1°C, 50 ppm, 0.8 MPa).

propanol as the solvent, the dielectric constants are similar, the degree of intermolecular reaction is comparable, and the peak intensities are also comparable; the characteristic peak of the bridging ethane group -CH_2-CH_2- in the BTESE precursor appears at 2855-2920 cm^{-1} (C-H stretching vibration peak) and 1280-1420 cm^{-1} (C-H bending vibration peak); the broad peaks concentrated at 3300 cm^{-1} are the stretching vibration peaks of the hydroxyl group (O-H) and the water adsorbed by the BTESE network. The appearance of these characteristic peaks indicates the successful synthesis of BTESE organosilica sols.

Different catalyst preparation of BTESE sol coating on the PA carrier can be observed in Figure 7(a). NH3 catalytic BTESE silicone coating in dry sol has great sol particles and cracks, and BTESE organic silicone sol in the spin coating process is not stable, as can be seen from the corresponding electron micrograph, BTESE organosilica sol prepared by NH3 catalysis. The NH3-catalyzed BTESE organosilica sol was the worst in terms of film formation. In contrast, as shown in Figure 7(b), and hydrochloric acid-catalyzed BTESE organosilica sol has a more uniform particle size, smoother coating, and further improved roughness.

3.3. Structural Characterization of BTESE/PA Composite Membrane. As shown in Figure 8 and Table 2, the surface C element content of the BTESE/PA composite membrane decreases from 67.21% to 30.13%, O element content increases from 19.55% to 34.93%, N element content decreases from 13.24% to 0%, and Si element content increases from 0% to 34.94%. Compared with the PA support body in the surface XPS spectra of the BTESE/PA composite membrane, two new Si2s and Si2p feature peaks appear at 153.21 eV and 100.97 eV, belonging to the BTESE organosilica network, while the feature peak N1s of the PA membrane support layer almost disappears. This confirms the presence of BTESE silicone coating on the PA surface.

As shown in Figure 9, the PEG retention rate gradually increases with the increase of PEG molecular weight. The retention rate of PEG200 in the PA membrane is very low, and when the molecular weight reaches 800 Da, the retention rate reaches more than 90%. It is inferred that the PA membrane can retain molecules above 800 Da. The molecular weight of BTESE silicone composite film was measured in 200-400 Da. The retention rate of BTESE silicone composite membrane was 87.51% for PEG200, 96.32% for

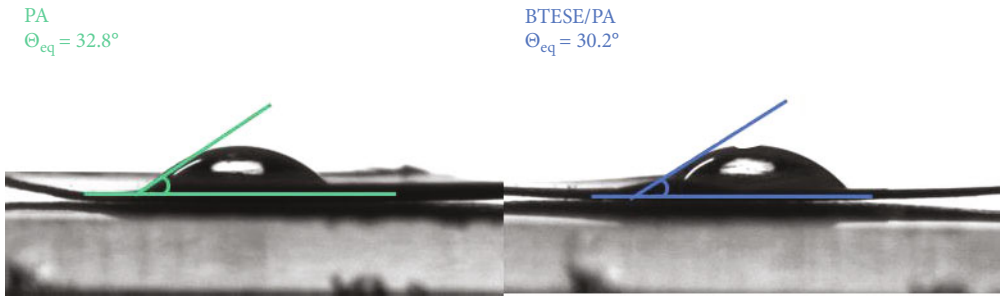

Figure 10: WCA of PA and BTESE/PA (PA, 5 wt% BTESE, 25 ± 1°C, 50 ppm, 0.8 MPa).

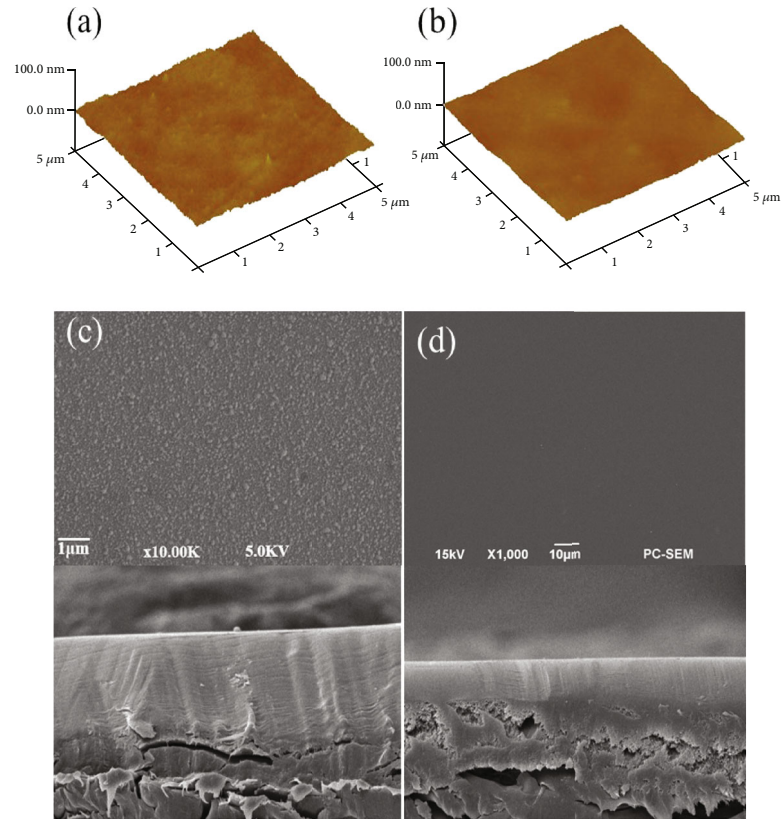

Figure 11: AFM and SEM of BTESE sol: (a, c) PA; (b, d) BTESE/PA.

PEG400, and 99.91% for PEG800. Therefore, through the interception molecular weight test of BTESE silicone composite film, the interception molecular weight of BTESE silicone composite film is between 200 and 400 Da.

By successfully loading the BTESE sol onto the PA spacer using a simple spin coating method, better surface hydrophilicity increases water permeability while maintaining a high retention rate. It can be seen in Figure 10 that the water contact angles of both PA and BTESE/PA films are less than 90°, which are hydrophilic film materials. The water contact angle of the composite membrane was reduced from 32.8°±2.1° to 30.2°±1.4°. The small water contact angle implies an increase in hydrophilicity, and the higher hydrophilicity also reduces the tendency of the membrane to organic scaling during the treatment of the PSMF solution.

The surface roughness and surface morphology of the membranes were assessed by atomic force microscopy (Nanoman VS). The surface roughness of the BTESE silicone composite membrane was observed in the scanning range of 5 μm × 5 μm, as shown in Figures 11(a) and 11(b). The surface of the uncomposite PA membrane was relatively rougher with a Ra value of 3.61 nm and further improved in roughness and uniformity compared to the BTESE/PA composite membrane with a Ra value of 2.30 nm. The surface and cross-sectional morphology of the BTESE/PA composite membrane were observed by field emission scanning

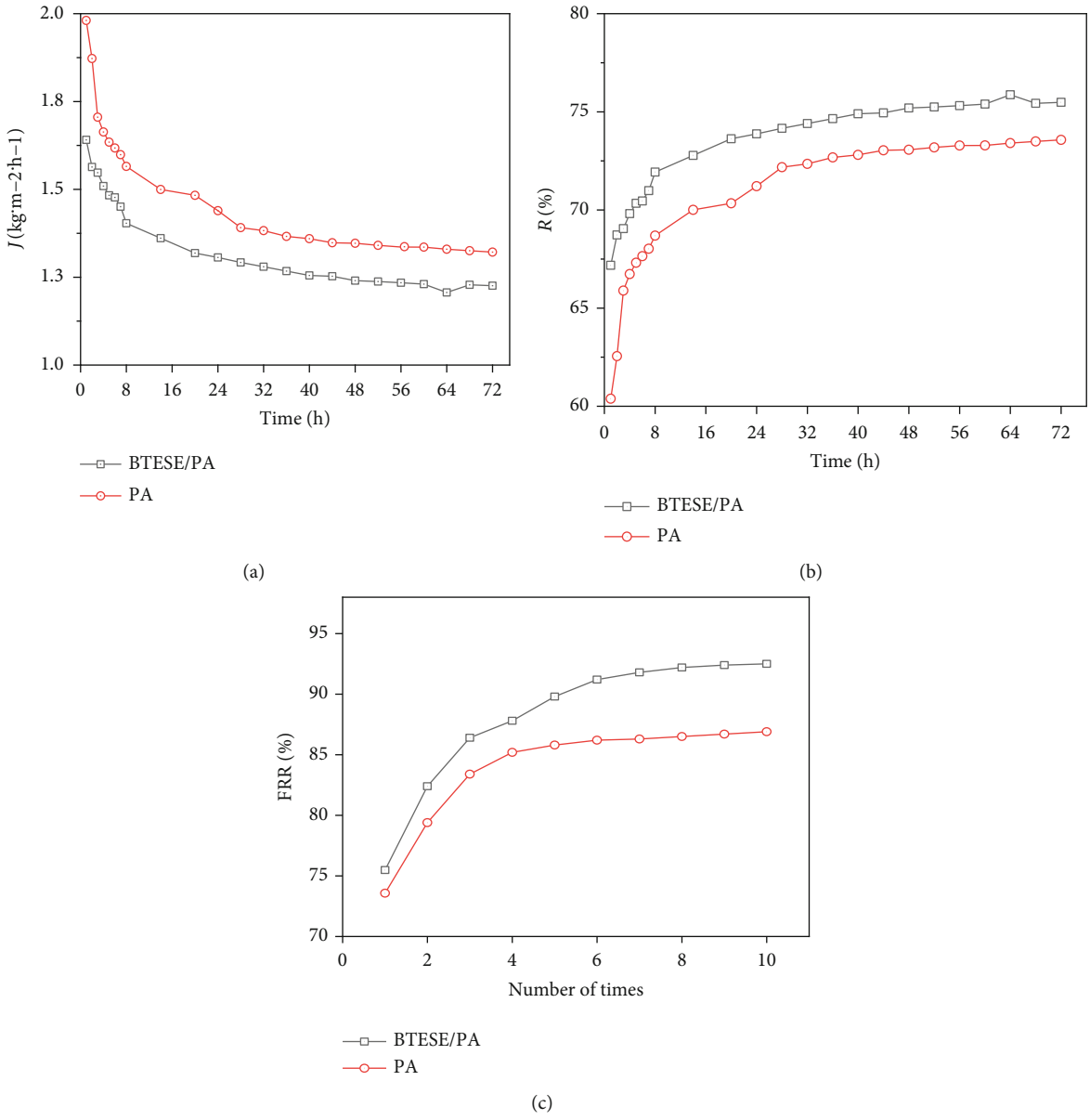

Figure 12: Separation performance of PA and BTESE/PA at 72 h: (a) membrane flux (J), (b) rejection rate (R), and (c) FRR.

electron microscopy (Zeiss, SUPRA 55), as shown in Figures 11(c) and 11(d). The surface and cross-sectional morphology of the BTESE/PA composite membranes are shown in Figures 11(c) and 11(d), where the surface of the BTESE/PA composite membrane is flatter and free of defects, while the BTESE silicone composite membrane is more brittle and broken in liquid nitrogen, and the BTESE particle layer, BTESE/PA separation layer, and support layer can be observed through the cross-sectional view. This is due to the in situ polymerization providing better dispersion of BTESE nanoparticle particles, reducing nanoparticle agglomeration and organic bridging of C-C, enhancing the compatibility between BTESE and PA structures, and preventing defects from occurring [38].

3.4. PSMF Membrane Separation before and after Performance Comparison. Figure 12 examines the separation performance of PA and BTESE/PA composite membranes in long-term operation. Under the transmembrane pressure difference of 1.0 MPa, the nanofiltration performance of BPA and BTESE/PA composite membrane was tested for 72 h, and the specific data are shown in Figures 12(a) and 12(b). After continuous operation for 72 h, the PSMF flux of the BTESE/PA composite membrane prepared by HCl was about 1.23 $kg \cdot m^{-2} \cdot h^{-1}$, and the retention rate was 75.48%. With the extension of the operation time, the retention rate increased by about 3% between 20 and 72 h, indicating that the surface of the BTESE/PA composite membrane was polluted, the mass transfer resistance on the surface of the membrane increased, the flux decreased, and the retention increased. The results show that the 72 h BTESE silicone composite membrane has long-term stability. The separation performance of the membrane is affected by membrane scaling over time. The permeable flux of the

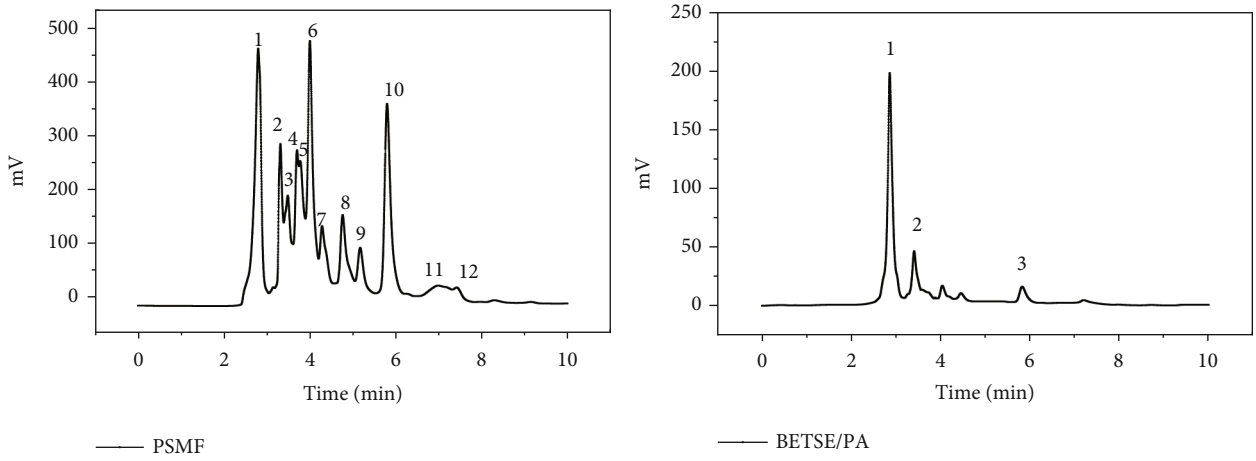

Figure 13: HPLC diagram of before and after PSMF separation.

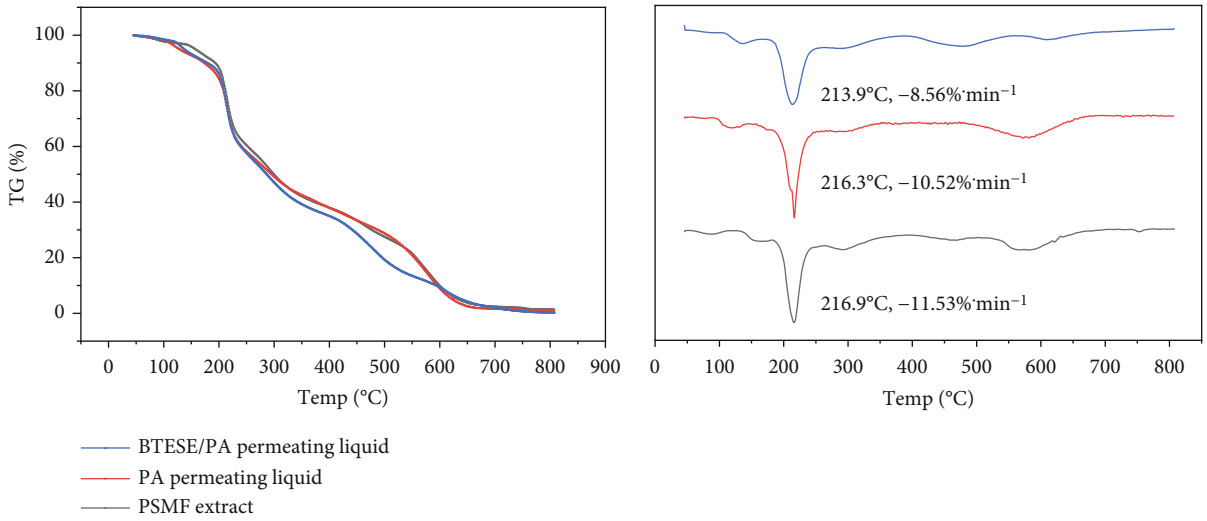

Figure 14: TGA spectra of extraction solution, permeation solution, and membrane passing solution (5 wt% BTESE, 25°C).

membrane can be reduced by several mechanisms, such as the adsorption of pollutants in the membrane pores, accumulation of pollutants on the membrane surface, and pore plugging. The hydrophobicity of the membrane surface may lead to poor antifouling performance. The membrane flux recovery rate of the BTESE/PA composite membrane is shown in Figure 12(c). After cleaning with pure water, the FRR of BTESE/PA was improved to some degree. After six times cleaning, the FRR of BTESE/PA was all greater than 90%, which was higher than that of the PA membrane, indicating that the antiscaling ability of BTESE/PA was better than that of the PA membrane. This may be related to the fact that the water contact angle of the BTESE/PA composite membrane is smaller than that of the PA membrane, and it also indicates that BTESE/PA composite membrane has better performance of separating PSMF than PA membrane.

The PSMF extract and the BTESE/PA composite membrane permeate were analyzed by high-performance liquid chromatography, and the experimental results are shown in Figure 13. The PSMF extract contained 12 flavonoid components, with fractions 1, 6, and 10 having a higher content. After separation by BTESE/PA composite membrane, the permeate contained 3 flavonoid substances, mainly the fractions at 2.85 min, and the content was reduced compared to the content in the PSMF extract. Therefore, the BTESE/PA composite membrane prepared in the laboratory has a good separation effect on the flavonoids in peony seed meal.

The thermal stability of PSMF extract, microfiltration membrane permeate, and BTESE/PA composite membrane permeate was characterized by using a thermogravimetric analyzer (NETZSCH, 209 F3) with a temperature rise rate of 10°C-min^{-1} and a temperature range of 50 to 800°C, operating under N_2 atmosphere, respectively. As can be seen in Figure 14, the thermal weight loss curve shows little change until 100°C, indicating that the extracts are stable and the materials do not thermally decompose until 100°C; between 100°C and 210°C, the thermal weight loss curve begins to show a slow decline, indicating that the material

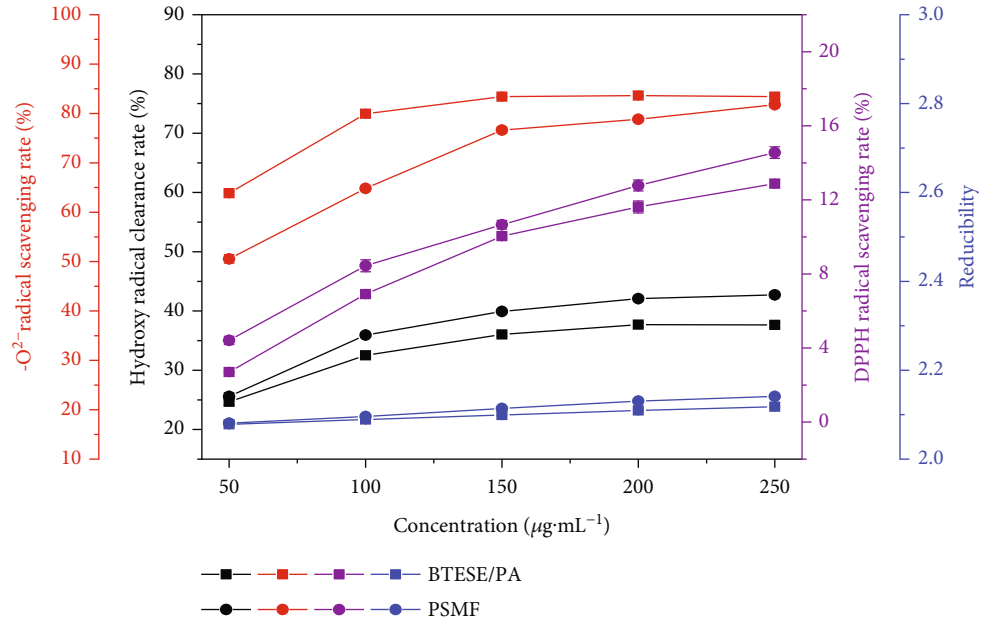

Figure 15: Schematic diagram of oxidation resistance of PSMF and membrane passing solution.

decomposition temperature and the phenomenon of thermal decomposition begin to appear, with a sample weight loss of approximately 5%; between 210°C and 280°C, the thermal weight loss curve decreases substantially, and most of the samples are thermally decomposed. The weight loss of the samples is about 42%, and the weight loss rate of the three substances reaches the maximum at this time, where the weight loss rate of PSMF extract > PA through liquid > BTESE/PA composite membrane through liquid weight loss rate, as compared to the increased thermal stability of the flavonoid extracts through the BTESE/PA composite membrane; after 280°C, the decreasing trend of the thermal weight loss curve decreases, for the thermal decomposition of the materials and ash. The residual masses of PSMF extract, microfiltration membrane permeate, and BTESE/PA composite membrane permeate after 800°C are 1.43%, 0.76%, and 0.26%, respectively, indicating that the residual ash of PSMF solution through BTESE/PA composite membrane has fewer impurities after heat and further suggesting that BTESE/PA composite membrane is more effective in separating the PSMF solution.

The semi-inhibitory concentration (IC_{50}) values of PSMF and BTESE/PA periplasmic solution were calculated by the following equation [31]:

$$\log IC_{50} = X_m - I\left[\frac{P - (3 - P_m - P_n)}{4}\right], \quad (7)$$

where X_m represents the logarithm of the maximum sample concentration, I refers to the logarithm of the ratio of the maximum sample concentration to the adjacent sample concentration, and P, P_m, and P_n stand for the sum of sample concentrations, the maximum sample concentration, and the minimum sample concentration, respectively.

In the measured concentration range, the membrane-filtered PSMF solution shows improved scavenging of -OH, superoxide anion, DPPH, and reducing power, specifically (in Figure 15), reducing power > -OH scavenging > DPPH scavenging, but the membrane permeate achieves lower $-O^{2-}$ scavenging than the PSMF raw solution. The IC_{50} (-OH) of PSMF is 0.19, the IC_{50} of BTESE/PA (-OH) is 0.18, and the -OH-clearance of BTESE/PA permuted solution is slightly higher than that of PSMF extract, probably because the membrane retained large molecules of impurities and small molecules of flavonoids passed through, and PSMF is rich in phenolic hydroxyl structure, so the clearance rate increases; the IC_{50} ($-O^{2-}$) of PSMF is 0.11, and theIC_{50}($-O^{2-}$ scavenging ability) is directly related to the phenolic hydroxyl group, which decreases when it is chelated by metal ions [39], and the o-diphenol structure in PSMF also inhibits $-O^{2-}$ scavenging; IC_{50} (DPPH) of PSMF is 0.16, and IC_{50} (DPPH) of BTESE/PA is 0.26. The scavenging mechanism of DPPH is dominated by H-atom transfer, so its scavenging curve is similar to that of -OH; the IC_{50} (reducing power) of PSMF is 0.14, and that of BTESE/PA is 0.42. The reducing power of PSMF permeate is slightly higher than that of the raw material solution, which may be due to the neutral nature of the permeated PSMF solution and the stability of the compound, which does not undergo self-oxidation. The reason for this may be that the PSMF solution is neutral, and the compound is stable and does not undergo self-oxidation, showing a strong scavenging ability that increases with the concentration of the compound.

The PSMF extract contained 12 natural flavonoids, and the BTESE/PA per membrane solution removed the large molecular impurities as well as the flavonoids with larger molecular weight. The per membrane solution had fewer flavonoids, so the antioxidant capacity decreased at the same concentration, but the free radical scavenging capacity was

increased with the increase in concentration. The results show that the BTESE/PA composite membrane has a good separation effect on the PSMF solution.

With the recognition of the efficacy of plant flavonoids in the European and American markets, the application of flavonoids is becoming more and more widespread, but the natural characteristic of flavonoids is their low water solubility, which limits the application of PSMF in functional beverages, cosmetics, and general food products [40]. Solutions filtered through PA and BTESE/PA membranes can effectively overcome this problem. The solubility is increased from 55.22% to 90.31%, and the water solubility of the filtered PSMF is significantly improved. The thermal stability after passing the membrane is good, and the food is thermally processed without destroying its biological activity, while still retaining some antioxidant activity for easy storage. The value of PSMF as a natural food additive should be valued and exploited, and the application of BTESE/PA organic nanofiltration membrane in flavonoid separation should be recognized.

4. Conclusion

In this study, five types of microfiltration membranes, namely, polypropylene (PP), polyvinylidene fluoride (PVDF), cellulose acetate (CA), polyethersulfone (PES), and polyamide (PA), were investigated. The effect of alkali acidity on the sols was investigated. The acid-catalyzed silicone sols increase the degree of condensation and crosslinking of the silicone network structure, resulting in a more stable structure, and the increase of C-C enhances the compatibility between BTESB and PA structure, preventing defects and improving the durability of BTESE/PA composite membrane. The spin coating method was used to coat the PA support to evaluate the effect of sol-gel on the composite membrane. The results from X-ray photoelectron spectroscopy, atomic force microscopy, and swept surface electron microscopy analysis revealed that the BTESE sol is successfully loaded on the PA spacer by using a simple spin coating method. The water contact angle of the composite membrane is reduced, and higher hydrophilicity also reduces the organic scaling tendency of the membrane when treating PSMF solution. In addition, the PSMF extract was treated with the permeate of the BTESE/PA composite membrane by the thermogravimetric analyzer, and the results show that the permeate has less residual ash and fewer impurities after being heated at 800°C. It can be inferred that the BTESE/PA composite membrane has a good filtration effect on the PSMF solution. The free radical scavenging ability of the solution before and after the separation of the composite membrane was measured, and the results further indicate that the BTESE/PA composite membrane has a better separation effect on the PSMF solution, and the purified solution has an improved scavenging ability on $\cdot O^{-2}$ free radicals.

However, the type of polymer and its compatibility plays an important role not only in terms of performance but also in the manufacture of the membrane. Although much progress has been made in the field, there is still an urgent need to work on enhancing the intrinsic properties of membrane surfaces, including hydrophilicity and electric surface charge, to improve the antifouling/biofouling and antibacterial properties of membranes. In addition, new researchers in the field are advised to analyze the separation performance and biofouling properties of the novel membranes using truly complex solutions, such as industrial by-products and wastewater. In this sense, the developed membranes can provide more realistic insights, which can clearly outline the potential of these membranes in water treatment applications.

Data Availability

The data used to support the findings of this study are included in the article.

Additional Points

Sample Availability. Samples of the compounds are available from the authors.

Conflicts of Interest

The authors declare that they have no known competing financial interests or personal relationships that could have appeared to influence the work reported in this paper.

Authors' Contributions

P.Z., R.X., and Y-Y.Z. contributed to this study. Y.X., W-T.C., and Y-H.W. were responsible for data collection. Y.X. and W-T.C. were responsible for data analysis and interpretation. Z.P., Y.X., W-T.C., Y-H.W., Y-Y.Z., and R.X. generated the manuscript.

Acknowledgments

This work was supported and funded by the Science and Technology Project of Jiangsu (no. BY2021215), Jiangsu Forestry Innovation and Promotion Project (LYKJ-CZ [2021]03), and Changzhou Sci&Tech Program (CE20225057).

Supplementary Materials

Supplementary materials for this study have been uploaded as attachments. *(Supplementary Materials)*

References

[1] R. Deng, J. Gao, J. Yi, and P. Liu, "Peony seeds oil by-products: chemistry and bioactivity," *Industrial Crops and Products*, vol. 187, no. 1, article 115333, 2022.

[2] Z.-Z. Bai, J.-M. Tang, J. Ni et al., "Comprehensive metabolite profile of multi-bioactive extract from tree peony (Paeonia ostii and Paeonia rockii) fruits based on MS/MS molecular networking," *Food Research International*, vol. 148, article 110609, 2021.

[3] R. Castro-Muñoz, E. Diaz-Montes, E. Gontarek-Castro, G. Boczkaj, and C. M. Galanakis, "A comprehensive review on current and emerging technologies toward the valorization

of bio-based wastes and by products from foods," *Comprehensive Reviews in Food Science and Food Safety*, vol. 21, no. 1, pp. 46–105, 2022.

[4] R. Castro-Muñoz, O. Garcia-Depraect, E. Leon-Becerril, A. Cassano, C. Conidi, and V. Fila, "Recovery of protein-based compounds from meat by-products by membrane-assisted separations: a review," *Journal of Chemical Technology and Biotechnology*, vol. 96, no. 11, pp. 3025–3042, 2021.

[5] R. Castro-Muñoz and V. Fíla, "Membrane-based technologies as an emerging tool for separating high-added-value compounds from natural products," *Trends in Food Science & Technology*, vol. 82, pp. 8–20, 2018.

[6] M. Zou, W. Zhang, R. Wu, H. Jiang, F. Cao, and E. Su, "Removal of ginkgo toxin from the Ginkgo biloba seeds powder by adopting membrane separation technology," *Journal of Cleaner Production*, vol. 280, no. 20, article 124452, 2021.

[7] A. Nazir, K. Khan, A. Maan, R. Zia, L. Giorno, and K. Schroën, "Membrane separation technology for the recovery of nutraceuticals from food industrial streams," *Trends in Food Science & Technology*, vol. 86, pp. 426–438, 2019.

[8] J. Zhang, Z. Tian, X. X. Ji, and F. Zhang, "Light-colored lignin extraction by ultrafiltration membrane fractionation for lignin nanoparticles preparation as UV-blocking sunscreen," *International Journal of Biological Macromolecules*, vol. 231, article 123244, 2023.

[9] H. Castricum, A. Sah, R. Kreiter, D. A. Blank, J. Vente, and J. E. ten Elshof, "Hydrothermally stable molecular separation membranes from organically linked silica," *Journal of Materials Chemistry*, vol. 18, no. 18, pp. 2150–2158, 2008.

[10] R. Xu, J. Wang, M. Kanezashi, T. Yoshioka, and T. Tsuru, "Development of robust organosilica membranes for reverse osmosis," *Langmuir*, vol. 27, no. 23, pp. 13996–13999, 2011.

[11] R. Erragued, M. E. Braga, M. Bouaziz, and L. M. Gando-Ferreira, "Integration of solvent extraction and membrane processes to produce an oleuropein extract from olive leaves," *Separation and Purification Technology*, vol. 299, no. 15, article 121751, 2022.

[12] R. Castro-Muñoz, J. Yáñez-Fernández, and V. Fíla, "Phenolic compounds recovered from agro-food by-products using membrane technologies: an overview," *Food Chemistry*, vol. 213, pp. 753–762, 2016.

[13] D. Pichardo-Romero, Z. P. Garcia-Arce, A. Zavala-Ramírez, and R. Castro-Muñoz, "Current advances in biofouling mitigation in membranes for water treatment: an overview," *Processes*, vol. 8, no. 2, p. 182, 2020.

[14] R. Xu, P. Lin, Q. Zhang, J. Zhong, and T. Tsuru, "Development of ethenylene-bridged organosilica membranes for desalination applications," *Industrial & Engineering Chemistry Research*, vol. 55, no. 7, pp. 2183–2190, 2016.

[15] R. Xu, Z. Lin, P. Lin, Q. Zhang, and J. Zhong, "Pervaporative desulfurization of model gasoline using PDMS/BTESE-derived organosilica hybrid membranes," *Fuel Processing Technology*, vol. 154, pp. 188–196, 2016.

[16] R. Xu, M. Guo, J. Wang, Q. Zhang, and J. Zhong, "Fabrication of solvent-resistant copolyimide membranes for pervaporation recovery of amide solvents," *Chemical Engineering & Technology*, vol. 41, no. 2, pp. 337–344, 2018.

[17] R. Xu, S. M. Ibrahim, M. Kanezashi et al., "New insights into the microstructure-separation properties of organosilica membranes with ethane, ethylene, and acetylene bridges," *ACS Applied Materials & Interfaces*, vol. 6, no. 12, pp. 9357–9364, 2014.

[18] M.-A. Pizzoccaro-Zilamy, C. Huiskes, E. G. Keim et al., "New generation of mesoporous silica membranes prepared by a Stöber-solution pore-growth approach," *ACS Applied Materials & Interfaces*, vol. 11, no. 20, pp. 18528–18539, 2019.

[19] M.-G. Yan, L.-Q. Liu, Z.-Q. Tang et al., "Plasma surface modification of polypropylene microfiltration membranes and fouling by BSA dispersion," *Chemical Engineering Journal*, vol. 145, no. 2, pp. 218–224, 2008.

[20] M. Mertens, T. Van Dyck, C. Van Goethem, A. Y. Gebreyohannes, and I. F. J. Vankelecom, "Development of a polyvinylidene difluoride membrane for nanofiltration," *Journal of Membrane Science*, vol. 557, pp. 24–29, 2018.

[21] L. C. Battirola, P. F. Andrade, G. V. Marson, M. D. Hubinger, and M. d. C. Gonçalves, "Cellulose acetate/cellulose nanofiber membranes for whey and fruit juice microfiltration," *Cellulose*, vol. 24, no. 12, pp. 5593–5604, 2017.

[22] E. Mansor, "Tight ultrafiltration polyethersulfone membrane for cheese whey wastewater treatment," *Chemical Engineering Journal*, vol. 407, article 127175, 2021.

[23] R. Dai, H. Han, T. Wang, J. Li, C. Y. Tang, and Z. Wang, "Fouling is the beginning: upcycling biopolymer-fouled substrates for fabricating high-permeance thin-film composite polyamide membranes," *Green Chemistry*, vol. 23, no. 2, pp. 1013–1025, 2021.

[24] L. Zan, W. Song, W. Wang, G. He, X. Li, and J. Pei, "Purification, antioxidant activities, encapsulation, and release profile of total flavonoids in peony seed meal," *Food Science & Nutrition*, vol. 10, no. 4, pp. 1051–1057, 2022.

[25] Y. Li, E. R. Thomas, M. H. Molina et al., "Desalination by membrane pervaporation: a review," *Desalination*, vol. 547, article 116223, 2023.

[26] P. Li, H. Xie, Y. Bi et al., "Preparation of high flux organic solvent nanofiltration membrane based on polyimide/Noria composite ultrafiltration membrane," *Applied Surface Science*, vol. 618, article 156650, 2023.

[27] L. Y. Ee, R. P. W. Tan, S. Y. R. Chia, and S. F. Y. Li, "Electrospray fabrication of anti-fouling nanocellulose desalination membrane with high flux," *Separation and Purification Technology*, vol. 322, article 124260, 2023.

[28] R. Wu, Y. Tan, F. Meng, Y. Zhang, and Y.-X. Huang, "PVDF/MAF-4 composite membrane for high flux and scaling-resistant membrane distillation," *Desalination*, vol. 540, article 116013, 2022.

[29] S. Liu, S. Keten, and R. M. Lueptow, "Effect of molecular dynamics water models on flux, diffusivity, and ion dynamics for polyamide membrane simulations," *Journal of Membrane Science*, vol. 678, article 121630, 2023.

[30] C. A. Smith, E. J. Want, G. O'Maille, R. Abagyan, and G. Siuzdak, "XCMS: processing mass spectrometry data for metabolite profiling using nonlinear peak alignment, matching, and identification," *Analytical Chemistry*, vol. 78, no. 3, pp. 779–787, 2006.

[31] J. Treml and K. Šmejka, "Flavonoids as potent scavengers of hydroxyl radicals," *Comprehensive Reviews in Food Science and Food Safety*, vol. 15, no. 4, pp. 720–738, 2016.

[32] J. Lu, Z. Huang, Y. Liu et al., "The optimization of extraction process, antioxidant, whitening and antibacterial effects of Fengdan peony flavonoids," *Molecules*, vol. 27, no. 2, p. 506, 2022.

[33] X. Chen, L. Liang, and C. Han, "Borate suppresses the scavenging activity of gallic acid and plant polyphenol extracts on

DPPH radical: a potential interference to DPPH assay," *LWT-Food Science and Technology*, vol. 131, article 109769, 2020.

[34] A. W. L. Andrade, K. da Conceição Machado, K. da Conceição Machado et al., "In vitro antioxidant properties of the biflavonoid agathisflavone," *Chemistry Central Journal*, vol. 12, no. 1, p. 75, 2018.

[35] Z. Jie, J. Liu, M. Shu, Y. Ying, and H. Yang, "Detection strategies for superoxide anion: a review," *Talanta*, vol. 236, article 122892, 2022.

[36] J. Zhu, L. Qin, A. Uliana et al., "Elevated performance of thin film nanocomposite membranes enabled by modified hydrophilic MOFs for nanofiltration," *ACS Applied Materials & Interfaces*, vol. 9, no. 2, pp. 1975–1986, 2017.

[37] G. Dong, H. Nagasawa, L. Yu et al., "Energy-efficient separation of organic liquids using organosilica membranes via a reverse osmosis route," *Journal of Membrane Science*, vol. 597, article 117758, 2020.

[38] L. Liu, F. McGain, and S. E. Kentish, "Recovery of sevoflurane anesthetic gas using an organosilica membrane in conjunction with a scavenging system," *Environmental Science & Technology*, vol. 55, no. 5, pp. 3362–3367, 2021.

[39] L.-M. Dong, X.-C. Jia, Q.-W. Luo et al., "Phenolics from Mikania micrantha and their antioxidant activity," *Molecules*, vol. 22, no. 7, p. 1140, 2017.

[40] V. D'Amelia, R. Aversano, P. Chiaiese, and D. Carputo, "The antioxidant properties of plant flavonoids: their exploitation by molecular plant breeding," *Phytochemistry Reviews*, vol. 17, no. 3, pp. 611–625, 2018.